An improved nanosatellite attitude control simulator for experimental research

Alex McCafferty-Leroux, Andrew Newton, S. Andrew Gadsden

Alex McCafferty-Leroux, Andrew Newton, S. Andrew Gadsden, "An improved nanosatellite attitude control simulator for experimental research," Proc. SPIE 12546, Sensors and Systems for Space Applications XVI, 1254607 (13 June 2023); doi: 10.1117/12.2675437

SPIE.

Event: SPIE Defense + Commercial Sensing, 2023, Orlando, Florida, United States

An Improved Nanosatellite Attitude Control Simulator for Experimental Research

Alex McCafferty-Leroux[a], Andrew Newton[a], and S. Andrew Gadsden[a]

[a]Department of Mechanical Engineering, McMaster University, Hamilton, Canada

ABSTRACT

This paper details the design, fabrication, and development of an improved Nanosatellite Attitude Control Simulator (NACS). The NACS consists of a mock 1U CubeSat (MockSat), tabletop air-bearing, and automatic balancing system (ABS). The MockSat employs a reaction wheel array to exchange momentum with the rigidly-attached air bearing platform, and an inertial measurement unit to obtain orientation and angular velocity estimates. The ABS tunes the Simulator's center of gravity to coincide with the air bearing's center of rotation in an effort to minimize gravitational torques. This paper presents the majority of the mechanical design process, as well as future insights into the ABS control system. The NACS will be used to build numerous data sets for the development and training of new machine learning algorithms, as well as to benchmark, test, and compare different estimation and control strategies.

Keywords: Attitude Control, CubeSat, Automatic Balancing System, Inertial Measurement Unit, Mechanical Design, Estimation

1. INTRODUCTION

As space exploration requirements increase and mission complexity advances, it becomes increasingly important to ensure a satellite's attitude determination and control system (ADCS) can operate under extreme and unexpected conditions. In scientific data collection, communication, and observation, it is required that satellite positioning is exceptionally accurate, where even brief inaccuracies can cause flawed data and signal dropout. For instance, deep space nanosatellites such as APEX [1] and Juventas [2] are heavily reliant on accurate attitude determination when measuring surface and form characteristics of asteroids. The livelihood of many on Earth can also be greatly affected by positioning errors, since these same systems are essential to the effectiveness of GPS satellites and climate monitoring systems. Using an arrangement of sensors, actuators, and well designed control algorithms, autonomy and robustness can be achieved in satellite maneuvering and stability.

The ADCS can be described as the unification of the attitude control and attitude estimation systems, which can facilitate the regulation of a satellite's state, track a trajectory, or perform a reorientation maneuver. The attitude control system (ACS) influences the state of the actuator and the satellite, whereas the attitude determination system (ADS) measures the environmental and vehicular states, attenuates noise, and updates global information for actuator reaction. Ideally, this data exchange and achieving the desired system states are performed with minimal error. The need for advanced control systems is therefore a necessary research area, ensuring satellites can function effectively and efficiently in stochastic environments.

The Nanosatellite Attitude Control Simulator (NACS), developed in the ICE Laboratory at McMaster University [3], contributes to this mission by aiming to study the effectiveness of control and estimation strategies for the CubeSat class of nanosatellites. A modular standard for fabricating economical and easily deployable satellites [4], the CubeSat program has enabled students and institutions to conduct meaningful scientific research on a relatively small scale. In particular, Dalhousie University's LORIS 2U CubeSat dedicated to coastline imaging and instrument testing [5] was successfully implemented, and McMaster University's recently launched NEUDOSE for studying the effects of long-term space radiation exposure [6] shows promising results. Operating in a

Further author information: (Send correspondence to A. McCafferty-Leroux or S. A. Gadsden)
A.M.L.: E-mail: mccaffea@mcmaster.ca
S.A.G.: E-mail: gadsden@mcmaster.ca

Sensors and Systems for Space Applications XVI, edited by Genshe Chen, Khanh D. Pham, Proc. of SPIE Vol. 12546, 1254607 · © 2023 SPIE
0277-786X · doi: 10.1117/12.2675437

broad spectrum of missions and various orbital altitudes, CubeSat research is undeniably essential to the future of space exploration. In its current state, the NACS has been developed to demonstrate state regulation and trajectory/target tracking using PID, feedback linearization (FBL) and sliding mode control (SMC) algorithms [3]. The simulator allows effective algorithmic research to be conducted for CubeSat in a laboratory setting, through the use of the automatic balancing table (ABS) and the experimental control stand.

Considering the observed performance of the ABS in [3], it was determined that it should be redesigned. Primarily due to malfunctioning and fundamentally limited electronics hardware, the X, Y, and Z axis balancing masses were required to be manually tuned at the beginning and during experiments. This resulted in several limitations to the experiment overall. Achieving automatic and highly-accurate tunability of all axes through the new ABS design would enable increased maneuver complexity and the ability to showcase the performance of various controller/estimation schemes. Additionally, the experimental stand will undergo a revision for purposes of support and streamlined data collection. The ABS and stand are expected to increase the functionality of the existing CubeSat system through these redesigns. The following body of the paper outlines the mechanical design process of the ABS and stand, with conclusions providing a trajectory for future research.

2. MECHANICAL DESIGN

2.1 Overview

The complete NACS experimental setup is comprised of the CubeSat Unit, the ABS, and the experimental stand. The unit is fixed to the ABS, which is attached to the upper portion of an air bearing. When activated, a thin layer of air forms between the air bearing sections, creating a frictionless cushion that the ABS and CubeSat can rotate about three axes on without resistance. The reaction wheel array of the CubeSat governs this movement, and the system center of mass (CoM) is driven to near coincidence with the air bearing center of rotation (CoR) through translational masses on the ABS. A mass on each Cartesian axis provides the ability to directly influence the system CoM in X, Y, and Z, to a limited degree. This mechanism removes body torques induced by gravity when the CubeSat is performing maneuvers, simulating a zero-gravity space environment. From the geometry of the complete air bearing, there is 360 degree rotation about the Z-axis (yaw), and +/- 30 degrees about the X and Y axes. To accommodate its range of motion, the air bearing must be elevated and rigidly fixed. The experimental stand design achieves this, as well as housing the functional and safety electronics, and the air circuit hardware. The system is supplied by a 100 psi air line for the air bearing, which is stepped down to 20 psi via a regulator. A solenoid valve is then utilized to remotely open and close the air circuit to perform experiments. In subsequent sections, the revised system will be presented and discussed in terms of design criteria and changes in performance.

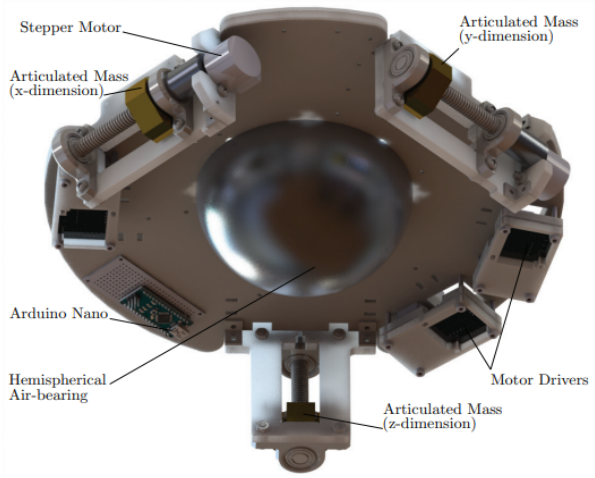

Figure 1. Previous ABS Design [3, pp. 23]

2.2 Automatic Balancing Table

As previously mentioned, it was crucial for the ABS to undergo a redesign due to its inability to achieve stability autonomously, since axial masses were translated manually (see Figure 1). This resulted in CoM coordination accurate to 0.5 mm [3, pp. 24]. Before starting the experiment, the ABS was tuned to reach an acceptable level of balance to define the initial conditions. However, because of this operation, there was always a few degrees of offset from the rotational origin, and the ABS could not reach a true steady state where the CoM was coincident with the CoR. This limitation would be compounded if the CubeSat was in motion, and therefore the CubeSat trajectories in the experiment had to be primarily limited to rotations about the Z axis, with small movement allowable (under 5 degrees) about the X and Y axes. This was a result of underperforming electronics hardware, which was improved upon in the revision. Additionally, the general form and several processes were reconsidered, as seen in Figure 2.

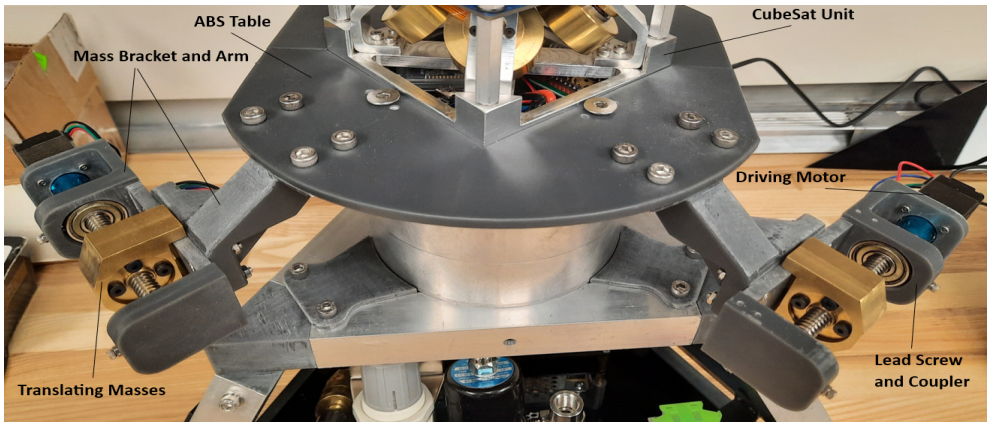

Figure 2. Labeled ABS System

For the ABS to be able to achieve stability autonomously, the stepper motors of each axis first had to be replaced. The milled brass masses were manufactured to be fastened to a flanged lead screw nut, which move along each axis of the CubeSat/ABS inertial frame through the shaft rotation of the associated stepper motor. Previously, the 28BYJ-48 4-phase stepper motor were used for this purpose, but proved ineffective due to step skipping, low step-resolution, and low operational torque [7]. The revised ABS must feature higher-resolution and higher torque motors, yet still be lightweight. This requirement is derived from the fact that the ABS and CubeSat system CoM must be a certain distance in each axis from the air-bearing CoR, where the masses can be adjusted to drive the CoM to that location if offset. If the system is unbalanced too much in any axis, it could be that no mass position achieves near CoM/CoR alignment. This was a major design consideration, where the geometry, material, and placement of every component of the ABS had to be considered and iterated upon. In terms of the motors, since they are located below the CoR, they cannot be so heavy such that the Z-axis mass is not able to drive the vertical axis CoM to the CoR. The ability of the revised ABS to achieve stability from its own form and the translational masses is verified below. The alignment of the CoR and the CoM is theoretically obtained from these equations as having the X, Y, and Z masses at 17.47, 18.78, and 23.27 mm on their respective axes. The Solidworks model was also used to verify the limits of the CoM vector in each major dimension, by translating each mass to the max and min of its motion. The resultant $\mathbf{r_{CM}}$ vector is approximately limited to exist within a 2 mm cube centered around the CoR.

$$0 = \frac{m_{b,1}\, x_1 + m_{b,2}\, x_2 + m_{b,3}\, x_3 + (m_{\text{sys}})\, x_{\text{static}}}{m_{\text{total}}} \rightarrow\ x_1 = -x_2 - x_3 - \frac{m_{\text{sys}}}{m_b}\, x_{\text{static}} \tag{1}$$

$$0 = \frac{m_{b,1}\, y_1 + m_{b,2}\, y_2 + m_{b,3}\, y_3 + (m_{\text{sys}})\, y_{\text{static}}}{m_{\text{total}}} \rightarrow\ y_2 = -y_1 - y_3 - \frac{m_{\text{sys}}}{m_b}\, y_{\text{static}} \tag{2}$$

$$0 = \frac{m_{b,1}\, z_1 + m_{b,2}\, z_2 + m_{b,3}\, z_3 + (m_{\text{sys}})\, z_{\text{static}}}{m_{\text{total}}} \rightarrow z_3 = -z_1 - z_2 - \frac{m_{\text{sys}}}{m_b}\, z_{\text{static}} \tag{3}$$

To assist in balancing the final design, weights were placed along the planar X-axis and the vertical Z-axis. The motors selected were the NEMA 8 stepper motors, which on their own feature 1.8 degrees/step (200 steps/revolution), an overall mass of 60 g, and an operating torque of 1.6 Ncm [8]. The ability of the motor to drive the masses under the most extreme loading case (vertical raising) is verified from Equation 4 below. This condition makes it so the motor must overcome the driven mass and friction. Additionally, the friction was reduced in the bearings to ensure the motors can drive the masses, choosing a sealed bearing design that used carbon steel instead of rubber as the shield.

$$T = \frac{W d_m}{2} \frac{f\ \pi\ d_m + L\ \cos\ \alpha_n}{\pi\ d_m\ \cos\ \alpha_n - f\ L} \tag{4}$$

The mass of the weight, lead screw nut, and fasteners were determined to be 136.4 g, resulting in a weight of 1.338 N (denoted W). An 8 mm diameter lead screw with a 2 mm pitch/lead was used, so $d_m = d - 0.5p = 7$ mm. The thread angle on the normal plane, α_n was defined as 29 degrees (ACME standard), and the unit-less friction coefficient applied was 0.15 [9]. The torque equation outlined was derived from [9, pp. 418]. The nominal torque required for the condition is 0.126 Ncm, which is lower than the motor torque of 1.6 Ncm.

The set of discrete locations obtainable by the translational masses relative to the lead screw is a function of the screw lead (translation/rev), the stepper motor step size (degrees), and the micro-stepping capabilities of the motor driver. To improve the resolution of the lead screw stroke (i.e., increase the number of locations the mass can be stationary within a finite distance), the enhanced micro-stepping capability of the TMC2209 stepper motor drivers was utilized. On its highest setting, these drivers can be tuned such that there are 256 subdivisions per step of the motor, which was earlier determined to be 1.8 degrees. This results in 51200 steps per revolution. The lead screw used has a pitch of 2 mm, so for the total stroke length of 48 mm, there are 1228800 possible locations for the mass. This indicates 39e-9 m of separation between locations for all masses, and is represented as $\Delta r_{i,b}$ (where its vector is of size 3 with identical entries). This is because the vector r_b for each mass has two constant entries and one variable entry, so the difference between the current and last position is simply the difference between the variable entries, or $\Delta r_{i,b}$. This is demonstrated with the variable x in Equation 5 below.

$$\Delta r_{x,b} = r_{b,k} - r_{b,k-1} = x_{b,k} - x_{b,k-1} \tag{5}$$

We can compute the accuracy of the alignment between the CoR and the CoM using this quantity and the ratio between the balancing mass and the total system mass [10]. Ideally, we would want the norm of this vector to be as small as possible. With Equation 6, we can conclude theoretically that the CoM can be tuned to the CoR within a vector of length 1.57 nm in all directions (or 2.72 nm).

$$\Delta \mathbf{r}_{\mathrm{CM}} = \frac{m_b}{m_{\mathrm{total}}} \Delta r_b \tag{6}$$

We can also compute the maximum residual torque as a result of gravity based on the accuracy vector (as used in [10]), from Equation 7. This quantity comes from the inability to perfectly align the gravity vector with the body Z axis, resulting in some minimal gravitational torque. The norm of the maximum torque vector was determined to be 7.3 x 10^{-8} Nm, but in real trials, it would likely be larger due to imperfections in the model [10], such as lead screw backlash, unmodelled disturbances from vibration, flexibility in the ABS platform, etc.

$$T_{\max} = \|\Delta \mathbf{r}_{\mathrm{CM}} \times \mathbf{g}\ m_{\mathrm{total}}\| \tag{7}$$

The range of motion of the ABS (and therefore the CubeSat Unit) is +/- 360 degrees about the Z axis, and +/- 30 degrees about the X and Y axes. This is not improved upon since the last design iteration, due to the geometry of the air bearing hemisphere and seat. Significant experiments can still be conducted in the lab with this limitation.

The structural components of the ABS are entirely 3D printed. Using SLA resin printing methods, we can achieve strong parts with complicated geometry at high resolutions. The Formlabs Tough 2000 [11] resin was used for all 3D printing operations, excluding the lower air-bearing mounting bracket (which was FDM printed in PLA) This includes the ABS table, the motor/mass brackets, and the ABS arms. Additionally, the system is designed such that it can be easily assembled and disassembled for hardware maintenance using fasteners. The mass/motor brackets for each axis are one piece, housing the lead screw and mass, the driving motor, the shaft coupler, and the limit switches, employed such that when an extreme is met the motor does not burn itself out trying to compensate an impossible CoM location. The brackets also feature a shielded channel for the limit switch and stepper signal wire organization. The wires are then fed to the arms, which connect the motor/mass brackets to the ABS table. They are located away from the CoR (and desired CoM, down and out) so that the translational masses have increased influence over the alignment. This has to do with the moment of inertia (MOI) tensor calculated about the reference frame (in this case, the CoR), and the mass distance from this origin. If the masses were coincident with the CoR, their movement would have a negligible contribution to the MOI, considering the size of the system. With the ABS arms, we are able to choose the amount of influence the masses have on the CoM during the design process, as well as ensure rigidity in movement. This can be observed in the fastener placement, as well as the triangular and thick-walled geometry. Additionally, the arms are hollowed for motor/limit switch wire management, feeding to the bottom of the ABS table, under the CubeSat, and into the air-bearing pocket.

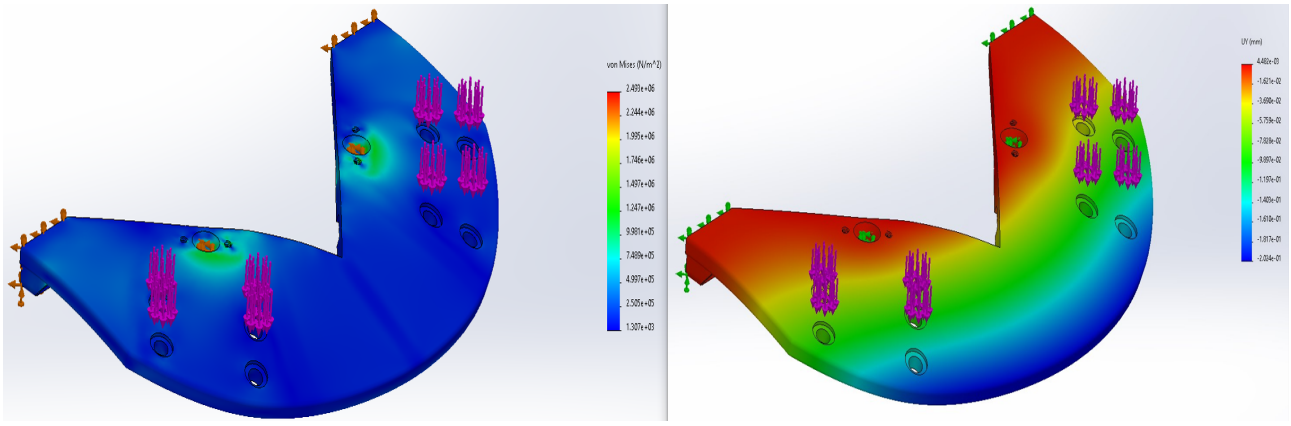

Figure 3. Von Mises Stress and Vertical Displacement Distribution of Loaded ABS Half

The ABS table connects the ABS arms to the air-bearing fixture holes, while also constraining the motion of the CubeSat while experiments are occurring. Designed as two separate parts to accommodate the printer's build volume, the ABS table is essentially a balanced plate with holes for fastening components and positioning the translational mass system further from the CoR. The ABS halves are flanged so that they can be fastened together. Additionally, ribbing was utilized in the table design. This was done for the purposes of saving material and thereby lowing the cost of this relatively large part. This does not compromise its rigidity and strength however, as they increase the bending stiffness of the plate [12]. The ribs are oriented radially outward from the center of the ABS (relative to the radius of the primary curve) to compensate for the loading it experiences from the translational mass sub-assemblies. The reduction of stress concentrations was also critical for the design of the ABS table, since the thickness is small (2.5 mm solid, 2.5 mm ribs). The design of the ABS was verified in Solidworks through a static loading simulation, as presented as Figure 3 above. The half with the most extreme loading condition (i.e. the half containing the X and Y motor assemblies) was simulated, presenting the vertical displacement of the table and the Von Mises stresses present.

The locations in which the ABS is fastened to the air-bearing and the other ABS table half were considered the fixed planes in the analysis. The load is distributed for each axis across the four mounting holes used by the arms, so normal forces of magnitude 1 N were applied at these locations. The weight of the ABS arms and motor assembly for each axis is approximately 3.4 N, so the 1 N loading at each hole serves as a small safety factor. The material of the SLA resin used was approximated using the ABS material pre-loaded in Solidworks [13].

It was determined that the maximum vertical displacement was 0.2 mm downward, and the maximum stress experienced is approximately 1.5 MPa (at the air-bearing mounting holes). These results are acceptable and demonstrate that the part will not fail, even under unexpected loading conditions, having a yield strength of 48 MPa [14]. The design should also ensure sufficient rigidity, as to not induce vibrations in movement, influencing the translation of the masses and controllability of the CoM.

Efficiently packed in the hemispherical air-bearing are the power and control electronics of the ABS system. Pictured below in Figure 4, this organization method is an alternative to the previous, where the electronics were located along the ABS table (Fig. 1). The form factor of the electronics was minimized through selective orientation and alternative choices in motor drivers and boost converter. Additionally, the motors, drivers, microcontroller, and Bluetooth receiver/transmitter are powered by a single lithium polymer (LiPO) battery, as opposed to three 9 V cells individually powering each motor. The length of time the ABS can be used before re-charging increases and power allocation is therefore streamlined. An additional change between the previous and current ABS iterations is that instead of employing an additional IMU for the ABS, the ABS uses the VN-100 IMU onboard the CubeSat Unit, since they are considered to be rigidly fixed. This reduces computational and electrical system complexity considerably for the ABS. The configuration of the electronics is visualized below. Under the maximum 3A that the system can possibly draw at a time, the 850 mAh battery is able to last 17 minutes from a full charge, which is significantly longer than the estimated experiment duration of 2 minutes [3, pp. 78].

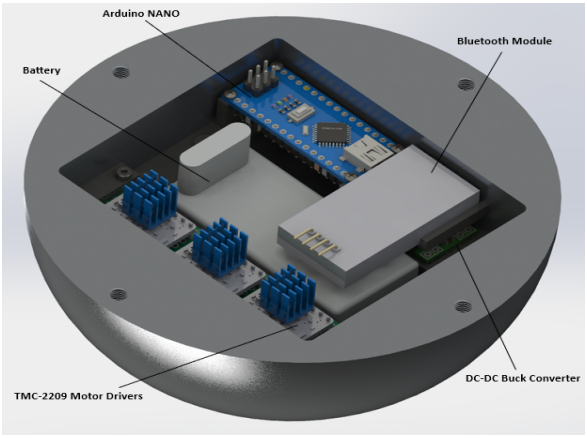

Figure 4. ABS Electronics Enclosure

2.3 Experimental Stand

The improved experimental stand offers several improvements over its previous iteration. Essentially a tall cylinder, it fit the outer diameter of the bottom portion of the air-bearing and offered little stability, since its caster wheels were arranged along a diameter that was smaller than the stand form diameter. The revised stand was designed with rigidity and streamlined experimentation in mind. This is achieved through the design of an aluminum frame with the experimental control and safety electronics contained within the setup.

The experimental stand presents a rigid design, safety features, and an efficient process for collecting data and starting experiments. The form of the stand was designed to be triangular for increased structural support, using hollow square aluminum 6061 1-inch profiles. The stand could not also be so large that it does not fit on a lab bench or cannot be moved easily. The primary contributor to the system weight is the CubeSat Unit (approx. 1.1 kg), and the upper and lower portions of the air bearing (approx. 3.5 kg). The profiles were cut to length and assembled using 3D printed brackets, which utilized pin joining to the profiles. The brackets were designed to secure the profiles in place with no wobbling, to support the system, and to nullify the requirement of angled cuts on the profiles. The rigidity design factor is important for support, but also significantly reduces the vibration from the surrounding environment being imposed on the system, increasing observed state accuracy and controller effectiveness. The top portion of the frame allows for the secure mounting of a 3D-printed cuff for the lower portion of the air bearing. The constructed stand is presented below in Figure 5.

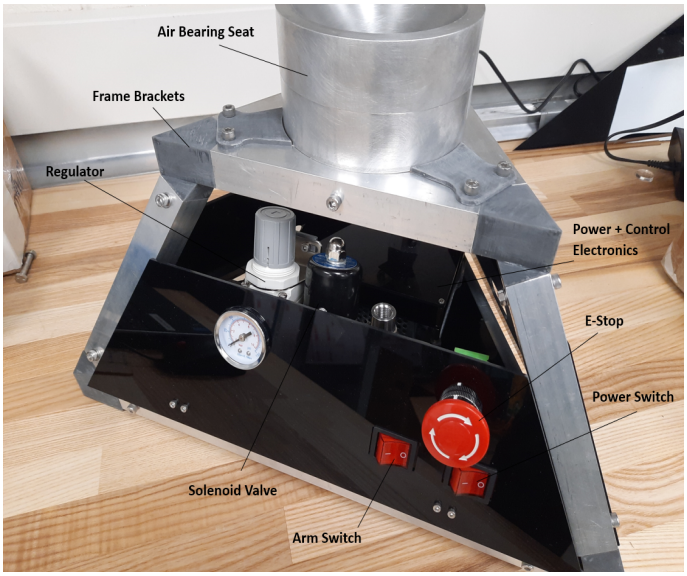

Figure 5. Labeled Experimental Stand

The controllable air circuit and multi-step experiment enabling system are important additions that improve the overall safety and handling of the system. Previously, the air supply (100 psi) had a shutoff valve that can be manually switched before the hose inlet, where it passed through the regulator to step the pressure down to 20 psi, and then to the air bearing. The experiment start and stop was dictated by this manual shutoff valve. Changing facilities, the air supply is at the opposite end of the lab from the experimental setup, making this procedure impractical and dangerous. The addition of the controllable air circuit makes it so that to start an experiment, the shutoff valve for the supply must be open and the normally closed solenoid must be electronically triggered such that it becomes open, letting air pass. To open the valve, the enabling system comes into play, where the power must be on and the system must be armed. Both safeguards are enabled/disabled with rocker switches. The setup computer must lastly send a signal to the stand microcontroller to start an experiment. An emergency stop button is also employed, completely shutting off system power if pressed. Additionally, the regulator, solenoid, and 1/4" NPT piping is rated for a significant safety factor over the operating pressure of the system.

The experimental stand streamlines the collection of data from CubeSat experiments, uploading automatically the attitude, reaction wheel velocity and torque, and the body velocity states to the setup computer. The onboard computer of the CubeSat (Raspberry Pi 3A+) measures all of these states during the experiment, and transfers the data to the stand micro-controller from the embedded Bluetooth receiver/transmitter. The data is then transferred by USB to the setup computer, so it can be organized and processed. The direct exportation of data enables simple categorization for later analysis, as well as database construction for possible machine learning (ML) applications (demonstrated in [15,16]).

2.4 Actuators and Sensors in CubeSat

The CubeSat unit being used for control and estimation research utilizes a redundant-pyramidal reaction wheel configuration [17, pp. 152 - 166] to achieve rotational stability about three axes. The reaction wheels govern the motion of the CubeSat in the setup, where four brushless DC motors are used to exchange momentum with the system. The redundancy is able to account for partial actuator system failure, since each motor is not solely responsible for its own axis. The Maxon Flat-EC 3W external rotor motors for the reaction wheels have Hall sensors, and are being used in conjunction with the ESCON 24/2 four-quadrant motor driver. This allows us to have full control over both the magnitude and direction, in speed and torque [18]. It can be seen in the satellite dynamics derived in the next section that this is vital for controllability. For this experimental setup, we are assuming that the satellite is operating in deep space, and as such does not utilize passive stabilization methods typically used by satellites to reduce energy expenditure (such as magnetic or aerodynamic) [19]. Additionally,

the effects of reaction wheel saturation will not be mitigated using momentum dumping [20, pp. 311]. This is applied when the motors achieve maximum velocity, and therefore do not contribute torque or momentum to the system, since it is built up in the reaction wheels. Typically, a magnetorquer is used for this occurrence, but saturation will be addressed for the conducted experiments with short run time, not allowing the motors to saturate. The reaction wheels of the NACS are the only actuation system used to achieve rotational stability.

To sense the CubeSat attitude, a VectorNav Rugged VN-100 IMU module is utilized. Using three axes of accelerometers, gyroscopes, and magnetometers, the attitude of the spacecraft (in Euler angles and quaternion) are accurately obtained, and then true states are estimated with an Extended Kalman Filter (EKF) [21]. Additionally, a Raspberry Pi 3A+ is used for computing, and all processes of the CubeSat are powered with onboard batteries. A labeled schematic of the CubeSat unit and the full assembly is presented below.

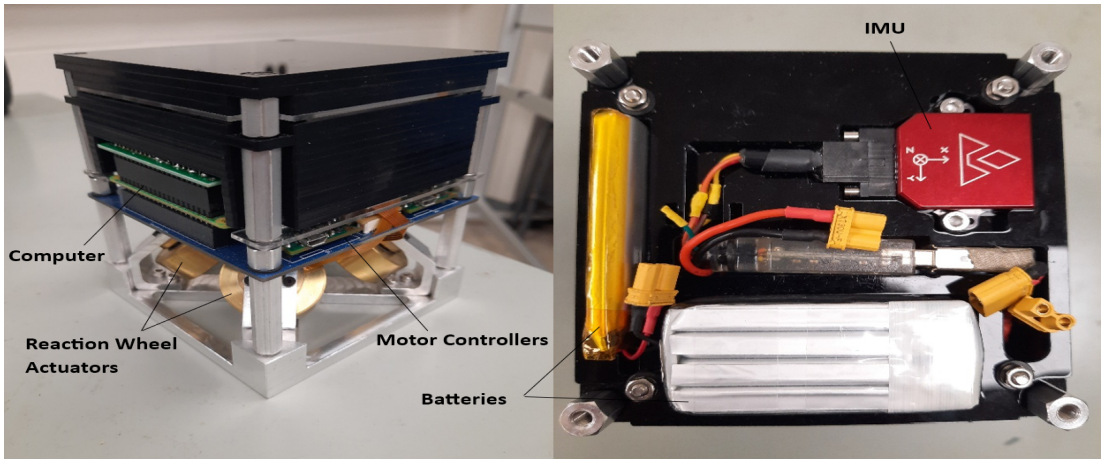

Figure 6. Mock 1U CubeSat Unit [3]

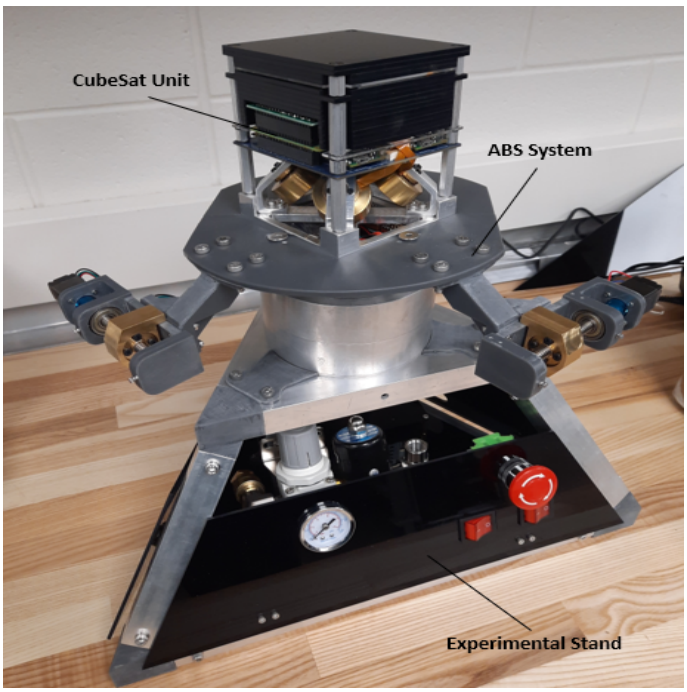

Figure 7. NACS Experimental Setup

3. CONCLUSIONS

The Automatic Balancing System of the NACS experimental setup is a key component used for testing Mock CubeSat attitude control algorithms in a lab setting. In an ideal situation, the ABS is able to tune the simulator's CoM to be coincident with the CoR of the platform air bearing, which in turn minimizes the amount of gravitational torque imposed on the CubeSat. This aspect of the ABS coupled with the frictionless rotation in three axes facilitates a pseudo-space environment. The paper explores the mechanical design process of the improved NACS experimental setup in detail, focusing on a complete form redesign, compactness, and safety. This includes the ABS and experimental stand revision. The mechanical analysis of the system validates its future completion and projected improved performance.

Overall, significant progress has been made on the construction of the ABS. However, for CubeSat attitude control laws to be tested in future research, the automatic balancing algorithm must still be implemented. This will facilitate the approximate alignment of the CoR and the CoM through the movement of the balancing masses, ensuring the system is able to maintain a desired attitude. The system dynamics and control scheme of this program can first be validated via computational experiment. Then, the microcontroller of the ABS must be able to have access to the measured data of the IMU, for the real time, physical implementation.

REFERENCES

[1] J. Wahlund, T. Kohout, D. Andrews, A. Penttila, "Asteroid Prospection Explorer (APEX) CubeSat for the ESA Hera Mission," *EPSC-DPS Joint Meeting*, vol. 13, Sept. 2019

[2] H. R. Goldberg, et al., "The Juventas CubeSat in Support of ESA's Hera Mission to the Asteroid Didymos," *33rd Annual AIAA/USU Conference on Small Satellites*, 2019

[3] A. Newton, "Design, Development, and Experimental Validation of a Nanosatellite Attitude Control Simulator," M.A.Sc Thesis, Dept. of Mechanical Engineering, University of Guelph, Guelph, ON, Canada, 2021.

[4] A. Poghosyan and A. Golkar, "CubeSat evolution: Analyzing CubeSat capabilities for conducting science missions," *Progress in Aerospace Sciences*, vol. 88, pp. 59-83, Nov. 2016, doi: 10.1016/j.paerosci.2016.11.002

[5] Dalhousie Space Systems Lab, *The LORIS Project - 2021*, dalorbits.com.
URL: https://dalorbits.ca/2019/07/01/loris-2021/ (accessed March 19, 2023)

[6] McMaster NEUDOSE, *McMaster NEUDOSE - CubeSat for Dosimetry of Charged and Neutral Particles*, mcmasterneudose.ca.
URL: https://mcmasterneudose.ca/ (accessed March 19, 2023)

[7] Kiatronics, *28BYJ-48-5V Stepper Motor*, mouser.com.
URL: https://www.mouser.com/datasheet/2/758/stepd-01-data-sheet-1143075.pdf (accessed March 26, 2023)

[8] Oyo Stepper, *Nema 8 Stepper Motor*, oyostepper.com.
URL: https://www.oyostepper.com/images/upload/File/8HS15-0604S.pdf (accessed March 26, 2023)

[9] R.C. Juvinall and K. M. Marshek, "Threaded Fasteners and Power Screws", *Fundamentals of Machine Component Design*, 5 ed. Hoboken, NJ, USA: John Wiley & Sons, Inc. 2012, ch. 10

[10] A. Bahu and D. Modenini, "Automatic Mass Balancing System for a Dynamic CubeSat Attitude Simulator: Development and Experimental Validation," in *CEAS Space Journal*, vol. 12, pp. 597-611, 2020, doi: 10.1007/s12567-020-00309-S

[11] Formlabs, *Tough 2000*, formlabs.com.
URL: https://formlabs-media.formlabs.com/datasheets/2001340-TDS-ENUS-0P.pdf (accessed March 26, 2023)

[12] Dienamics, *All About Ribs in Product Design*, dienamics.com.
URL: https://dienamics.com.au/blog/ribs-product-design/ (accessed March 26, 2023)

[13] Formlabs, *Using Tough 2000 Resin*, formlabs.com.
URL: https://support.formlabs.com/s/article/Using-Tough-Resin (accessed March 26, 2023)

[14] The Engineering Toolbox, *Thermoplastics - Physical Properties*, engineeringtoolbox.com.
URL: https://www.engineeringtoolbox.com/physical-properties-thermoplastics-d_808.html (accessed March 26, 2023)

[15] S. M. Sharun, M. Y. Mashor, W. N. Hadani, M. N. Norhayati, S. Yaacob, "Nano-Satellite Attitude Control System Based on Adaptive Neuro-Controller," from *Proceedings of the 3rd International Conference on Computing and Informatics, ICOCI*, no. 78, June 2011, Bandung, Indonesia

[16] R. Xie and A. G. Dempster, "An on-line deep learning framework for low-thrust trajectory optimisation," in *Aerospace Science and Technology*, vol. 118, doi: 10.1016/j.ast.2021.107002

[17] F.L. Markley and J.L Crassidis, "Sensors and Actuators," in *Fundamentals of Spacecraft Attitude Determination and Control*, New York: Springer, 2014, ch. 4

[18] Maxon, *ESCON Module 24/2 Servo Motor Controller*, maxongroup.com.
URL: https://www.maxongroup.com/maxon/view/news/MEDIARELEASE-ESCON-MODULE-24-2-ENCOM (accessed March 26, 2022)

[19] S. A. Rawashdeh, "Passive Attitude Stabilization for Small Satellites," M.A.Sc Thesis, Graduate School of the University of Kentucky, University of Kentucky, Lexington, KY, USA, 2010.

[20] F.L. Markley and J.L Crassidis, "Attitude Control," in *Fundamentals of Spacecraft Attitude Determination and Control*, New York: Springer, 2014, ch. 7

[21] VectorNav, *VN-100*, vectornav.com.
URL: https://www.vectornav.com/products/detail/vn-100 (accessed March 26, 2022)

[22] A. Bahu and D. Modenini, "Automatic Mass Balancing System for a Dynamic CubeSat Attitude Simulator: Development and Experimental Validation," in *CEAS Space Journal*, vol. 12, pp. 597-611, 2020, doi: 10.1007/s12567-020-00309-S